JTTEE5 12:112-119
© ASM International

Peer Reviewed

Characterization of Thermal Sprayed Nanostructured WC-Co Coatings Derived From Nanocrystalline WC-18wt.%Co Powders

Z.-G. Ban and L.L. Shaw

(Submitted 12 June 2001; in revised form 9 September 2001)

Nanostructured WC-Co coatings were synthesized using high velocity oxygen fuel (HVOF) thermal spray. The nanocrystalline feedstock powder with a nominal composition of WC-18 wt.%Co was prepared using the novel integrated mechanical and thermal activation (IMTA) process. The effects of HVOF thermal spray conditions and powder characteristics on the microstructure and mechanical properties of the as-sprayed WC-Co coatings were studied. It was found that the ratio of oxygen-to-hydrogen flow rate (ROHFR) and the starting powder microstructures had strong effects on decarburization of the nano-coatings. Decarburization was significantly suppressed at low ROHFR and with the presence of free carbon in the powder. The level of porosity in the coatings was correlated with the powder microstructure and spray process conditions. The coating sprayed at ROHFR = 0.5 exhibited the highest microhardness value (HV_{300g} = 1077), which is comparable to that of conventional coarse-grained coatings.

Keywords decarburization, high velocity oxyfuel thermal spray, microhardness, nanostructured coatings, nanostructured WC-Co

1. Introduction

In thermal sprayed WC-Co coatings, the hard WC particles act as the wear-resistant part, while the cobalt binder provides toughness and support. As a result of their excellent properties, thermal sprayed WC-Co coatings have been widely used in many industrial applications requiring abrasion, sliding, fretting, and erosion resistance.[1-3] Air plasma spraying (APS) and high velocity oxygen fuel (HVOF) spraying are the most common spray techniques used for preparing WC-Co coatings. HVOF thermal spraying has been proved to be a better method than APS for retaining a larger fraction of WC and reducing porosity, owing to lower temperatures and higher kinetic energy experienced by the powder particles.[4-6]

Recently, it has been reported that a bulk nanostructured WC-Co material exhibits higher hardness, toughness, and abrasion resistance than the conventional counterpart.[7,8] It has also been found that thermal spraying using nanostructured feedstock powder has yielded coatings with higher hardness, strength, and corrosion resistance than the corresponding conventional coating in some material systems such as Cr_3C_2-25(Ni20Cr)[9]and Ni.[10] From these results, it is anticipated that better mechanical properties may be achieved in thermal sprayed WC-Co coatings if nano-phase powder feedstock is used. However, until now, work on coatings has largely been restricted to the spraying of coarse-grained WC-Co powder feedstock and little work has been done in the area of nanostructured WC-Co coatings.[11-14] One reason for this is that development of nano-phase WC-Co powders is still in the initial stage, although the WC-Co powders containing 70-250 nm size WC grains synthesized using the spray conversion process have recently become commercially available.[15] The cost and the end-product powder characteristics such as hollow and porous microstructures, however, are hurdles for wide applications of the nano-phase WC-Co powders in the thermal spraying process.

Recently, nanostructured WC-Co composite powders have been successfully synthesized in our laboratory using a novel process termed the integrated mechanical and thermal activation (IMTA) process.[16-18] The efficacy of the IMTA process has also been demonstrated in producing pure nanostructured carbides (e.g., SiC and TiC)[19-22] and nitrides (e.g., Si_3N_4, CrN, and TiN).[23-25] The basic form of the IMTA process in making nanostructured WC-Co powders is to mechanically activate reactants WO_3, CoO, and graphite at room temperature through high energy milling (the mechanical activation step), followed by completing the synthetic reaction at high temperatures (the thermal activation step). The distinct feature of the IMTA process is the utilization of low cost materials while producing nanostructured WC-Co powder that has better powder characteristics (e.g., solid particles rather than hollow ones). Furthermore, the amount of free carbon present in the composite powder can be precisely tailored in the IMTA process to prevent decarburization during thermal spraying.

This article focuses on the characterization of thermal sprayed nanostructured WC-Co coatings derived from nanocrystalline WC-Co powders that are obtained using the IMTA process. The effects of HVOF thermal spraying conditions and powder characteristics on the microstructure and mechanical properties of the as-sprayed WC-Co coatings are highlighted.

Z.-G. Ban and **L.L. Shaw,** Department of Metallurgy and Materials Engineering, Institute of Materials Science, University of Connecticut, Storrs, CT 06269. Contact e-mail: lshaw@mail.ims.uconn.edu.

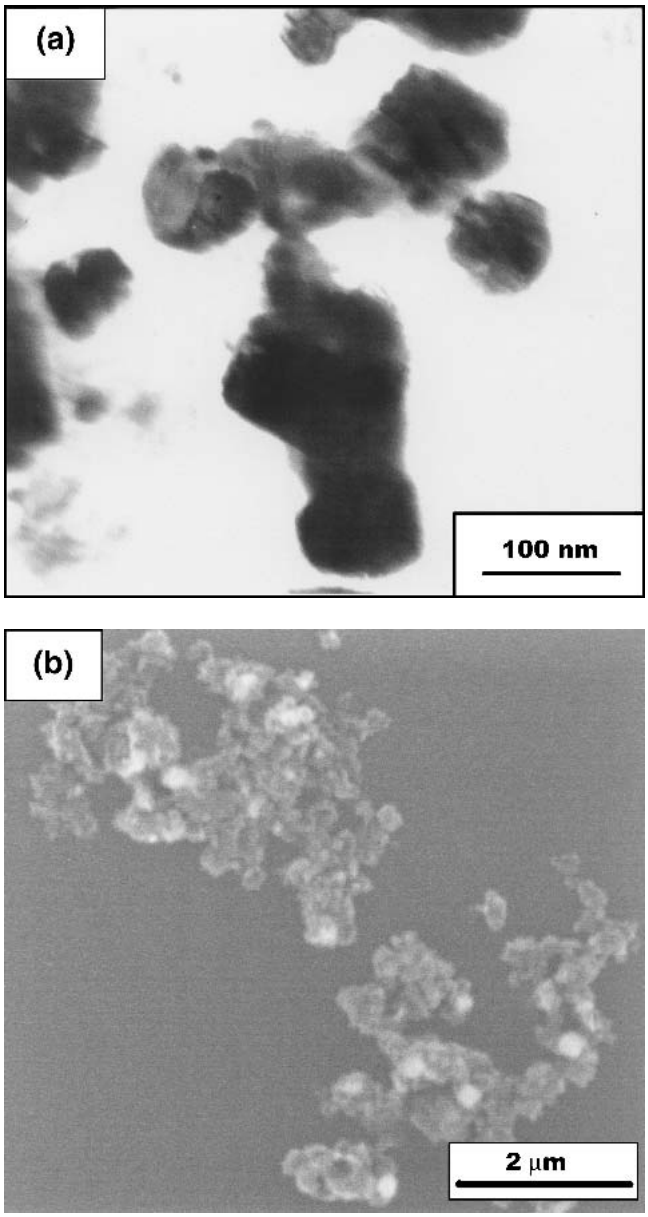

Fig. 1 **(a)** TEM and **(b)** SEM image of the WC-Co powder synthesized via the IMTA process

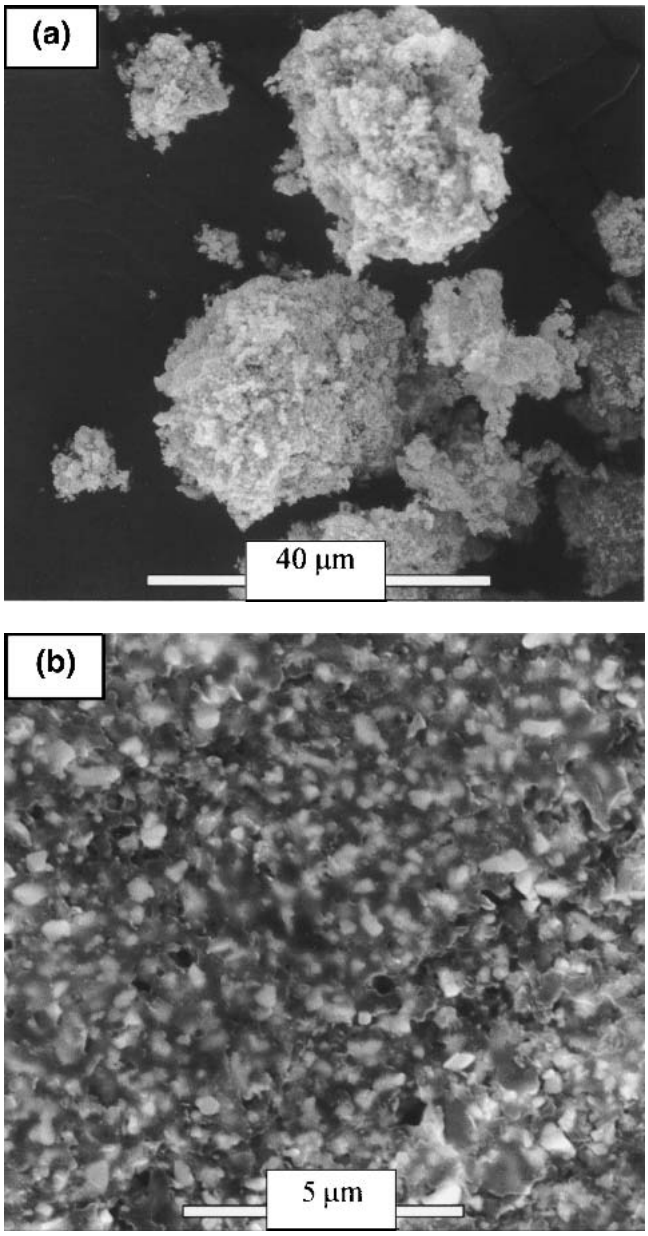

Fig. 2 SEM images of **(a)** the agglomerated particles and **(b)** the cross section of one agglomerate

2. Experiments

2.1 Feedstock Powder

Nanostructured WC-Co powder was synthesized using the IMTA process. The detail of this process can be found elsewhere.[16-18] The powder had a nominal composition of WC-18 wt.%Co+5.3 wt.%C (free carbon) with particle sizes ranging from 0.3-0.5 μm and an average WC grain size around 30 nm as revealed with transmission electron microscopy (TEM) (Fig. 1a), scanning electron microscopy (SEM) (Fig. 1b), and the peak broadening of x-ray diffraction (XRD) patterns (not shown here). Thus, these WC-Co powders can be characterized as submicrometer-sized particles with nanograins.[16] Typically, the majority of the materials with HVOF systems have a particle size ranging from 10-50 μm. Thus, the WC-Co powder synthesized using the IMTA process is not suitable for thermal spraying. For this reason, the submicrometer-sized WC-Co powder particles were agglomerated to satisfy the size requirement of thermal spraying using methyl cellulose as the organic binder.[9,13] Figure 2 shows SEM images of the agglomerated particles and the cross section of one agglomerate. The size distribution of the agglomerated powder is in the range of 5-45 μm, with the majority of agglomerates measuring around 20 μm. It is clear from Fig. 2(b) that within the agglomerate the submicrometer-sized WC-Co particles are bonded together by the organic binder. The resulting WC-Co agglomerates are then suitable for subsequent HVOF thermal spraying.

Table 1 Parameters Employed During HVOF Spraying

Spray Parameter	Value
Powder feed rate	20 g/min
Spraying distance	0.2 m
Oxygen pressure	0.687 MPa
Hydrogen pressure	0.687 MPa
Ratio of O_2 to H_2 flow rate (ROHFR)	0.3, 0.5, and 0.6

2.2 HVOF Experiments

Deposition of the nano-phase WC-Co cermet powder was done using a commercial Jet-Kote gun (Stellite Coatings, Goshen, IN), HVOF thermal spraying system. Low carbon mild steel was used as the substrate material in this study. The substrate pieces were cut to 30 × 15 × 3 mm coupons and grit blasted right before deposition. The spray gun was mounted on automated gun handling equipment that could move the gun horizontally, as well as vertically, at chosen speeds. The spraying distance was 0.2 m and hydrogen was used as the fuel gas with argon as the powder carrier gas. In this study, spraying parameters were kept constant except for the ratio of the oxygen-to-hydrogen flow rate (ROHFR). Three different ROHFR (i.e., 0.6, 0.5, and 0.3) were evaluated and other spraying parameters are summarized in Table 1.

2.3 Coating Characterization

The phase identification of powder feedstock and as-sprayed coatings were carried out employing the Bruker AXS D5005D x-ray diffractometer with CuK_α radiation (Bruker Analytical X-ray Systems, Inc., Madison, WI). The average grain sizes of powders and coatings were determined based on XRD peak broadening using the Scherrer formula without consideration of internal strain.[26] Since the internal strain is not considered in this case, the estimated grain size could be smaller than the real size. However, the difference should be small, as we have found from the XRD peak broadening and TEM examination of the starting WC-Co powder synthesized via the IMTA process.[16] Morphology of the coating cross section was examined utilizing the Philips environmental SEM 2020 (Philips Electron Optics, Eindhoven, The Netherlands). The coating porosity was measured using the point counting method on the photograph of the coatings taken via a Nikon Metaphot optical microscope (Don Santo Corporation, Wellesley Hills, MA) under 600× magnification.[27] Vickers microhardness tests were performed using a LECO DM-400FT hardness tester (LECO Corporation, St. Joseph, MI). A 300 g load and the dwell time of 20 s were used for all the samples, except for the coating sprayed at ROHFR = 0.3, for which a 50 g load was used owing to the low thickness of the coating. For each coating sample, 5 indentations were made in the middle of the coating cross section parallel to the coating/substrate interface. The microhardness value reported is the average of 5 indentations.

3. Results and Discussion

3.1 Phases of the As-Sprayed Coatings

Figure 3 shows XRD patterns of the powder before spraying and the coatings sprayed at various ROHFR. It is clear that additional crystalline reflections, corresponding to W_2C and W phases, are present in all the coatings in comparison with the x-ray pattern of the powder. For the coating sprayed at ROHFR = 0.3, only traces of W_2C and W phases are detectable. With an increase in ROHFR, the peaks corresponding to W_2C and W become more pronounced, reflecting the increased degree of decarburization. Another distinct feature of XRD patterns for the coatings is the absence of the Co phase. Moreover, all of the patterns for the coatings in Fig. 3 show a broad diffraction halo between 2θ values of approximately 37 and 47°. It has been reported that this broad, shallow peak is associated with the formation of amorphous and/or nanocrystalline phases containing tungsten, cobalt, and carbon.[28-30] The fact that the cobalt peaks are detected in the powder particles and not in the coatings suggests that most of the cobalt in the coatings is retained in the amorphous and/or nanocrystalline phases.

Grain sizes of the coatings estimated on the basis of x-ray line broadening are given in Fig. 4. It is apparent that the WC grain size increases only slightly during thermal spraying. This result indicates that nanostructured WC-Co coatings were obtained. This result is also consistent with the fact that the low temperature and short dwell time that the powder particles experience during HVOF thermal spraying help to preserve the nanocrystalline structure in the final coatings.[10] Also, note from Fig. 4 that the grain size of WC in the coatings increases with increase of ROHFR. This may be attributed to the higher flame temperature associated with the higher ROHFR.[5]

The issue that needs to be addressed in thermal spraying of WC-Co coatings is often the formation of new phases, such as W_2C, W, and even WO_3 in the coatings.[5] The present XRD result (Fig. 3) clearly indicates the formation of W_2C and W in the as-sprayed coatings, although no WO_3 is detected. Moreover, the contents of these new phases depend strongly on ROHFR. It is generally agreed that three mechanisms may contribute to the formation of these new phases in thermal sprayed WC-Co coatings. In addition, all three mechanisms are accompanied by the global carbon loss in the system, thereby resulting in decarburization of WC-Co coatings.

Mechanism I is the peritectic decomposition of WC through the reaction:

$$2WC = W_2C + C \quad \text{(Eq 1)}$$

This reaction is responsible for the formation of W_2C in the plasma sprayed WC-Co coatings, as proposed by Vinayo et al.[31] However, computer simulations of HVOF processes have shown that under the typical HVOF spraying conditions the WC-Co particle temperature is normally below the WC peritectic decomposition temperature (2785 °C)[32] for the particle sizes ranging from 10-40 μm in diameter.[12] Fincke et al.[6] used a high speed two-color pyrometer to measure particle temperatures during the HVOF spraying and found that the particle temperatures were indeed below the WC peritectic decomposition temperature. Therefore, decarburization due to the peritectic decomposition of WC is negligible in the HVOF thermal spraying process, or at least it is not a dominant factor.

Mechanism II is the direct oxidation of WC to W_2C and subsequently W_2C to W. As the powder particles traverse from the gun exit to the substrate and then deposit on the substrate until they are covered by other particles, they will encounter signifi-

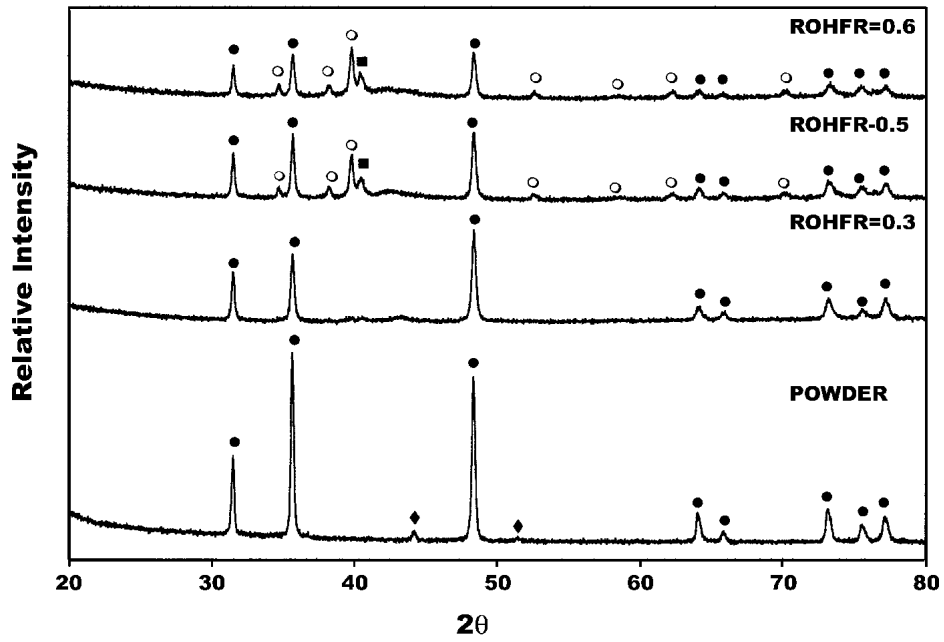

Fig. 3 XRD patterns of the powder and nanostructured coatings thermally sprayed at various ROHFR. WC, ●; Co, ♦; W_2C, o; W, ■

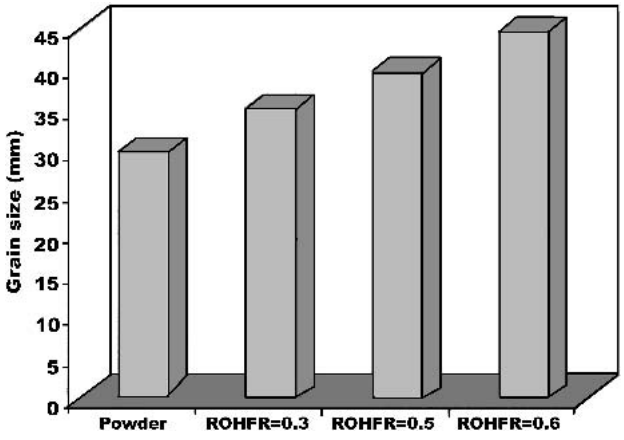

Fig. 4 Grain sizes of the powder and the as-sprayed coatings calculated from the peak broadening in the XRD patterns

cant oxygen levels in HVOF spraying.[33] The oxygen comes from the incomplete combustion reaction between oxygen and hydrogen and the air entrained into the jet from the atmosphere.[34,35] Accordingly, WC particles may react directly with the adjacent oxygen during flight or in the deposited state, forming thermodynamically favored W_2C phase, and subsequently, W phase through the following reactions, as suggested by Nerz et al.:[4]

$$4WC + O_2 = 2W_2C + 2CO \quad \text{(Eq 2)}$$

$$2W_2C + O_2 = 4W + 2CO \quad \text{(Eq 3)}$$

These proposed decarburization reactions in HVOF spraying are different from those in plasma spraying in which the particle temperature is high and the peritectic decomposition is mainly responsible for the decomposition of WC to W_2C, while the direct oxidation is mainly responsible for further decarburization from W_2C to W.[31]

Mechanism III is the dissolution of WC in the liquid Co matrix. In the dissolution process, the higher the liquid temperature, the more WC will dissolve. According to the liquidus surface projection calculated by Guillermet,[36] molten Co in equilibrium with WC could contain 50-60 wt.%W and 3-3.5 wt.%C at 2273 K. Furthermore, the solubility of tungsten and carbon in cobalt follows a reciprocal relationship (i.e., more tungsten with less carbon and vice versa).[37] Carbon could be removed from the melt either by reaction with oxygen at the melt/gas interface or through oxygen diffusion into the rim of the molten particle, leading to the formation of carbon monoxide. Therefore, the dissolution process is enhanced by the presence of oxygen. Due to the greater surface-to-volume ratio of nano-WC grains, mass transfer of carbon and tungsten into the Co-rich melt in nanostructured powders is remarkably faster than in conventional coarse-grained powders. For this reason, dissolution is accelerated for the nanocomposite particles. Another result of the dissolution is the formation of W_2C. Verdon et al.[29] suggested that the preferential dissolution of C could lead to the transformation of WC to W_2C with C diffusing away to the liquid Co (with or without its subsequent loss by oxidation). This argument is largely driven by the fact that W_2C rims are formed around WC grains. However, a recent study shows that the no duplex W_2C/WC grains were found in nanophase WC-Co coatings.[12] This result suggests that the WC phase may be completely dissolved and replaced by fine scale W_2C at elevated temperature owing to the enhanced dissolution of the nano-WC grains.

Although the direct oxidation and dissolution processes are the major mechanisms responsible for the decarburization of WC in HVOF spraying, it is difficult to separate the role of one

mechanism in total decarburization from another and clearly define the extent to which these two mechanisms occur. Generally, the direct oxidation mechanism affects only those WC grains at the gas/particle interface, whereas the dissolution mechanism affects the decomposition of WC grains at the subsurface of the particle.[12] In addition, the leading decarburization mechanism may change from one to another during the microstructure evolution in the thermal spraying process. For example, it might be expected that, upon melting, Co would wet the WC grains, thus preventing the direct contact of the WC grain with the gas phase. As a result, the dominant decarburization mechanism would change from the direction oxidation to dissolution.

On the basis of the decarburization mechanisms discussed above, the decarburization behavior of the nano-coatings sprayed at various ROHFR can be explained as follows. At the condition of ROHFR = 0.3, the goal to suppress decarburization of the nano-coating is realized (Fig. 3). The reason is that at this condition there is either no unburned oxygen or very little, if any, since ROHFR = 0.3 is below stoichiometry value (0.5).[32] Furthermore, the free carbon present in the powder can react with oxygen in the flame. The sacrificial reaction of free carbon with oxygen could consume some oxygen adjacent to the WC particles, thereby preventing WC from oxidation to a certain degree.[38] Moreover, the flame temperature is relatively low at this condition. As a result, the dissolution process is also slow. Thus, at ROHFR = 0.3 both the direct oxidation and dissolution processes are suppressed**.** With increasing ROHFR (in our case 0.5 and 0.6), more and more unburned oxygen is introduced. Consequently, it is possible that the free carbon present in the powder particles is consumed by oxidation quickly and not enough to suppress decarburization of WC. In addition, the temperature that the nano-powder particles experience will increase as a result of the larger enthalpy input with the increase of ROHFR,[5] leading to the acceleration of the dissolution process. Thus, significant amounts of W_2C, and even W, are present in the coatings sprayed at ROHFR = 0.5, and even more amounts in the coating sprayed at ROHFR = 0.6**.**

3.2 Coating Microstructures

Figure 5 shows the secondary electron image of the cross sections of the coatings thermally sprayed at various ROHFR. Microstructural characteristics of the three coatings can be summarized as follows.[1] There are two distinct regions: the fully melted and solidified region (type I region in Fig. 5b), and the partially melted and liquid phase sintered region (type II region in Fig. 5b).[2] The percentage of these two regions is a function of ROHFR (i.e., the volume fraction of the liquid phase sintered region increases with decreasing ROHFR).[3] Both the solidified region and liquid phase sintered region have splat morphology at ROHFR = 0.5 and ROHFR = 0.6. However, splat morphology becomes hard to discern when the coating is sprayed at ROHFR = 0.3, suggesting that at ROHFR = 0.3 the viscosity of the agglomerate is high when the agglomerate impinges on the substrate.

One of the major concerns in the coating microstructure is porosity, since it is correlated with the mechanical properties of the coating. Certain levels of porosity (>4%) were observed for all three coatings (Fig. 6). For the coating sprayed at ROHFR = 0.3, even microcracking is present. Note that owing to the resolution limit of the optical microscope, the contribution from the nano-sized voids to the total porosity could not be determined.

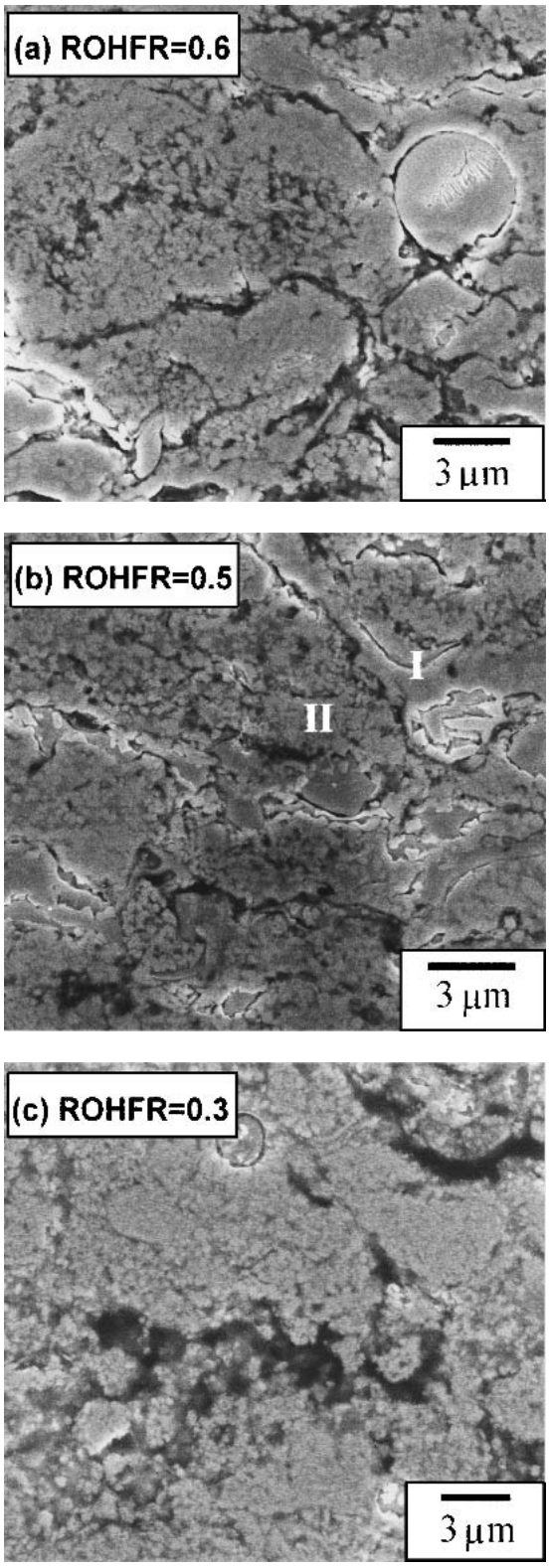

Fig. 5 Secondary electron images of the cross section of the coatings thermally sprayed at various ROHFR

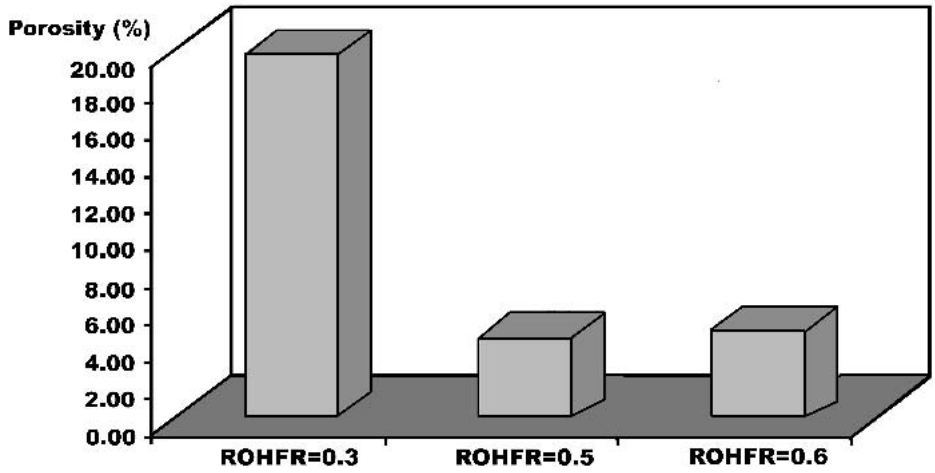

Fig. 6 The porosity of the coatings sprayed at various ROHFR

As a result, the data presented in Fig. 6 are only an approximation of the true porosity of the coatings. Normally, two types of porosity in the coatings can be defined in terms of their locations: one within the individual splat, and the other between the splats. The porosity within the splat is essentially related to the inherent powder porosity that is not always eliminated by thermal spraying, particularly in the HVOF process where powder particles are not usually fully melted.[5] It can be seen from Fig. 2(b) that the agglomerated powder particle contains considerable inherent porosity. In addition, the organic binder in the agglomerate will vaporize upon exposure to the high temperature field during the flight, thereby leaving behind porosity in the agglomerate. The formation of porosity between the splats is mainly influenced by the flame temperature and the powder particle velocity, which are basically controlled by ROHFR. As the flame temperature increases, more liquid matrix is formed. When the particle travels faster, the liquid matrix will tend to spread out in the substrate more easily due to the increasing impact force of the particle on the substrate. The combined consequence is that porosity between the splats in the coating will be much less at the condition of high flame temperature and high powder particle velocity. Thus, the level of porosity in the as-sprayed coatings could be explained as follows. At ROHFR = 0.3, the possibility of forming a large quantity of porosity between splats is relatively high owing to the low flame temperature and low particle velocity. At the same time, the inherent porosity present in the agglomerate is hard to eliminate due to the low spray temperature and velocity. Thus, the inherent powder porosity and, in particular, the porosity between splats result in a high level of porosity in the coating sprayed at ROHFR = 0.3. At ROHFR = 0.5 and 0.6, the porosity between the splats is easier to reduce due to the higher flame temperature and higher particle velocity than at ROHFR = 0.3. Similarly, the porosity within the splat is easier to reduce under high ROHFR conditions. Consequently, the total porosity resulting from the inherent powder porosity and the porosity between the splats are significantly lowered at these two ROHFR conditions.

3.3 Microhardness

Figure 7 summarizes Vickers microhardness of the coatings sprayed at three conditions. Mean values of the microhardness are 774 kg/mm^2 (HV_{50g}), 1077 kg/mm^2 (HV_{300g}), and 694 kg/mm^2 (HV_{300g}) for the coatings sprayed at ROHFR = 0.3, 0.5, and 0.6, respectively. The scatter of the hardness of the coating is the result of the intrinsic heterogeneity of the coatings, the anisotropy of the microstructure, and the small indentation size. For comparison, the published hardness data of conventional WC-12 and 17 wt.%Co coatings sprayed using HVOF are presented in Table 2. The Vickers microhardness HV_{300g} of conventional WC-Co coatings sprayed using HVOF is typically above 1000. The few results about the microhardness of nanostructured WC-Co coatings that have been published are summarized in Table 3, which indicates that the potential of high microhardness has not been demonstrated in the nanostructured WC-Co coating. It can be seen that the nanostructured coating sprayed at ROHFR = 0.5 in this study has the highest microhardness value (HV_{300g} = 1077) that is comparable to that of the conventional coatings and the nanostructured coatings reported from the literature. With either increasing or decreasing ROHFR, the microhardness of the coating drops off. The coating sprayed at ROHFR = 0.3, which has retained almost all the nano-WC grains during thermal spraying, does not show the expected high microhardness.

The factors that determine coating hardness are complex, and generally two factors are considered to be most important in determining the coating hardness: the volume fraction of the retained WC and the coating porosity.[3] Significant decarburization occurs in the nanostructured coatings sprayed at ROHFR = 0.5. As a result, the low volume fraction of the retained WC cancels the benefit of the small grain size, leading to no improvements in the hardness of the nanostructured coating. The increase of ROHFR further decreases the volume fraction of the retained WC, thereby lowering the microhardness of the coating, as occurred at ROHFR = 0.6. For the coating sprayed at ROHFR = 0.3, the high porosity is the main reason for the low hardness. As a result, the coating sprayed at ROHFR = 0.5 has the highest hardness among the three conditions studied.

The present microhardness result reveals that the spraying process has a strong effect on the coating properties. This is attributed to the fact that the spraying process could affect the volume fraction of the retained WC as well as the coating porosity (Fig. 3 and 6). Furthermore, the nanocomposite powders suffer greater levels of decarburization than the conventional coarse-

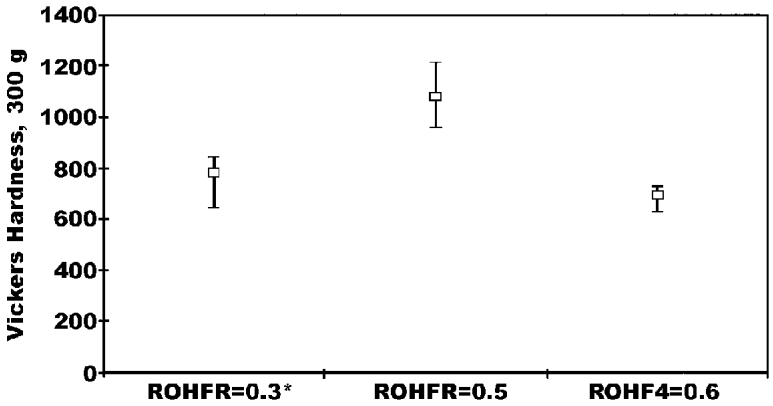

Fig. 7 Vickers hardness of the coatings sprayed at various ROHFR. ✷: Hardness was measured under a 50 g load, whereas the others were measured under a 300 g load.

Table 2 The Published Hardness Data of Conventional WC-Co Coatings Sprayed Using HVOF

Powder Composition	Gun Type	Fuel	Hardness, HV, 300gf
WC+17wt.%Co	self-constructed CH-2000 gun	propane	1000~1300(200gf)[37]
WC+17wt.%Co	Jet Kote	hydrogen	1080[39]
WC+17wt.%Co	Top Gun	hydrogen	1080[39]
WC+17wt.%Co	Jet Kote	propylene	1109[40](a)
WC+17wt.%Co	Jet Kote	propylene	1298[40](b)
WC+17wt.%Co	Top Gun	hydrogen	1136[15]
WC+12wt.%Co	JP-5000	kerosene	1060[41]
WC+12wt.%Co	Diamond Jet	propylene	1129[13]

(a) Cast & crushed powder
(b) Agglomerated powder

Table 3 The Published Hardness Data of Nanoscale WC-Co Coatings Sprayed Using HVOF

Powder Composition	Gun Type	Fuel	Hardness, HV, 300gf
WC+12wt.%Co	Diamond Jet	propylene	1135[13]
WC+15wt.%Co	Top Gun	hydrogen	1211[14]

grained powders due to the higher surface area per unit volume of particles. The transfer of the agglomerate porosity to the coating porosity also results in the difficulty in achieving fully dense coatings. Thus, the microstructure of the starting agglomerates is also one of the important factors affecting the coating properties. From these results it is reasonable to state that to fully realize potentials of the nanostructured WC-Co coatings, it is necessary to reduce the level of porosity in the agglomerated powder particle, minimize the exposure of the powder particle to oxygen, and reduce the level of entrained oxygen in the flame. Reducing the level of entrained oxygen in the flame could possibly be achieved by replacing the air shroud with an N_2 or argon shroud for entraining the flame, although the commercialization of this technique is still in doubt. To minimize the inherent powder porosity as well as the exposure of nano-particles to oxygen, the starting agglomerates may be heat treated before thermal spraying. With these improvements, it may be possible to obtain nanostructured WC-Co coatings with a low level of decarburization, dense microstructures, and improved properties.

4. Conclusions

- Nanostructured WC-Co coatings sprayed using HVOF thermal spraying have been obtained. The nanostructured WC-Co powder synthesized using the IMTA process can be used as the powder feedstock for generating nanostructured coatings.
- The ROHFR has strong effects on decarburization of the nano-coatings. The higher the ROHFR, the more W_2C and W phases are formed. Decarburization is significantly suppressed at low ROHFR and with the presence of free carbon in the powder.
- Certain levels of porosity (>4%) have been observed for all the coatings. The powder characteristics, including the inherent porosity, the organic binder phase, as well as the spray conditions (i.e., ROHFR), play an important role on the formation of the porosity in the coatings.
- Among the three coatings, the one sprayed at ROHFR = 0.5 exhibits the highest microhardness value (HV_{300g} = 1077), which is comparable to that of conventional coatings. With either increasing or decreasing ROHFR, the microhardness of the coating drops off. The coating sprayed at ROHFR = 0.3, although retaining almost all the nano-WC grains during thermal spraying, does not show the expected high microhardness due to the high porosity level. The coating sprayed at ROHFR = 0.6, although containing low porosity, exhibits the lowest hardness in the current study due to the increased decarburization.

Acknowledgments

The authors wish to thank Mr. Don Breakell and Mr. Cem Eminoglu from Sermatech International Inc., Manchester, CT for performing the spray runs and the National Science Foundation for the financial support under grant No. DMR-9710265.

References

1. S.F. Wayne and S. Sampath: "Structure/Property Relationships in Sintered and Thermally Sprayed WC-Co," *J. Therm. Spray Technol*., 1992, *1*(4), pp. 307-15.
2. H.J. Kim, Y.G. Kweon, and R.W. Chang: "Wear and Erosion Behavior of Plasma-Sprayed WC-Co Coatings," *J. Therm. Spray Technol*., 1994, *3*(2), pp. 169-78.
3. L. Pawlowski: *The Science and Engineering of Thermal Spray Coatings*, John Wiley & Sons, Chichester, England, 1995, pp. 210-74.
4. J. Nerz, B. Kushner, and A. Rotolico: "Effect of Deposition Methods on the Physical Properties of Tungsten Carbide-12wt.% Cobalt Thermal Spray Coatings" in *Protective Coatings: Processing and Characterization*, R.M. Yazici, ed., TMS, Warrendale, PA, 1990, pp. 135-43.
5. H.L. De Villiers Lovelock: "Powder/Processing/Structure Relationships in WC-Co Thermal Spray Coatings: A Review of the Published Literature," *J. Therm. Spray Technol.*, 1998, *7*(3), pp. 357-73.
6. J.R. Fincke, W.D. Swank, and D.C. Haggard: "Comparison of the Characteristics of HVOF and Plasma Thermal Spray" in *Thermal Spray Industrial Applications*, C.C. Berndt and S. Sampath, ed., ASM International, Materials Park, OH, 1994, pp. 325-30.
7. K. Jia and T.E. Fischer: "Sliding Wear of Conventional and Nanostructured Cemented Carbides," *Wear*, 1997, *203-204*, pp. 310-18.
8. K. Jia and T.E. Fischer: "Abrasion Resistance of Nanostructured and Conventional Cemented Carbides," *Wear*, 1996, *200,* pp. 206-14.
9. J. He, M. Ice, and E.J. Lavernia: "Synthesis of Nanostructured Cr_3C_2-25(Ni20Cr) Coatings," *Metall. Mater. Trans.,* 2000, *31A*(2), pp. 555-64.
10. M.L. Lau, H.G. Jiang, W. Nuchter, and E.J. Lavernia: "Thermal Spraying of Nanocrystalline Ni Coatings," *Phys. Stat. Sol. (a)*, 1998, *166*, pp. 257-67.
11. L.E. McCandish, B.H. Kear, B.K. Kim, and L.W. Wu: "Low Pressure Plasma-Sprayed of Nanophase WC-Co" in *Protective Coatings: Processing and Characterization*, R. M Yazici, ed., TMS, Warrendale, PA, 1990, pp. 113-19.
12. D.A. Stewart, P.H. Shipway, and D.G. McCartney: "Microstructural Evolution in Thermally Sprayed WC-Co Coatings: Comparison Between Nanocomposite and Conventional Starting Powders," *Acta Mater.,* 2000, *48*, pp. 1593-1604.
13. J. He, M. Ice, S. Dallek, and E.J. Lavernia: "Synthesis of Nanostructured WC-12 Pct Co Coating Using Mechanical Milling and High Velocity Oxygen Fuel Thermal Spraying," *Metall. Mater. Trans.*, 2000, *31A*(2), pp. 541-53.
14. D.A. Stewart, P.H. Shipway, and D.G. McCartney: "Abrasive Wear Behavior of Conventional and Nanocomposite HVOF-Sprayed WC-Co Coatings," *Wear*, 1999, *225-229*, pp. 789-98.
15. B.H. Kear and L.E. McCandish: "Chemical Processing and Properties of Nanostructured WC-Co Materials," *Nanostruct. Mater*., 1993, *3*, pp. 19-30.
16. L.L. Shaw, R-M. Ren, Z-G. Ban, and Z-G. Yang: "A Novel Process for Synthesizing Nanostructured WC/Co Powder" in *Powder Metallurgy Alloys and Particulate Materials for Industrial Applications*, D.E. Alman and J.W. Newkirk, ed., TMS, Warrendale, PA, 2000, pp. 75-80.
17. R-M. Ren, Z-G. Yang, and L.L Shaw: "Synthesis of Nanostructured WC/Co Powders Through an Integrated Mechanical and Thermal Activation Process," University of Connecticut, unpublished research.
18. Z-G. Ban and L.L. Shaw: "On the Reaction Sequence of WC-Co Formation Using an Integrated Mechanical and Thermal Activation Process," *Acta Mater*., 2001, *49*, pp. 2933-39.
19. L.L. Shaw, R-M. Ren, and Z-G. Yang: "Sinterable Carbides From Oxides Using High Energy Milling," U.S. Patent: 6 214 309.
20. R-M. Ren, Z-G. Yang, and L.L. Shaw: "A Novel Process for Synthesizing Nanostructured Carbides: Mechanically Activated Synthesis," *Ceram. Eng. Sci. Proc*., 1998, *19*(4), pp. 461-68.
21. R-M. Ren, Z-G. Yang, and L.L. Shaw: "Synthesis of Nanostructured TiC via Carbothermic Reduction Enhanced by Mechanically Activation," *Scripta Mater*., 1998, *38*(5), pp. 735-41.
22. L.L. Shaw: "Processing of Nanostructured Carbides, Nitrides and Their Composites," *Adv. Eng. Mater*., 2000, *2*(11), pp. 721-23.
23. L.L. Shaw, Z-G. Yang, and R-M. Ren: "Mechanically Enhanced Reactivity of Si for the Formation of Si_3N_4 Composites," *J. Am. Ceram. Soc*., 1998, *81*(3), pp. 760-64.
24. R-M. Ren, Z-G. Yang, and L.L. Shaw: "Synthesis of Nanostructured Chromium Nitride Through Mechanical Activation Process," *Nanostruct. Mater*., 1999, *11*(1), pp. 25-35.
25. R-M. Ren, Z-G. Yang and L.L. Shaw: "Nanostructured TiN Powder Prepared via an Integrated Mechanical and Thermal Activation Process," *Mater. Sci. Eng.,* 2000, *A286*, pp. 65-71.
26. H.P. Klug and L.E. Alexander: *X-ray Diffraction Procedures for Polycrystalline and Amorphous Materials*, John Wiley & Sons, London, UK, 1954, pp. 491-94.
27. G.F.V. Voort: *Metallography Principles and Practice*, McGraw-Hill Inc., New York, 1984, pp. 426-28.
28. C-J. Liu, A. Ohmori, and Y. Harada: "Effect of Powder Structure on the Structure of Thermally Sprayed WC-Co Coatings," *J. Mater. Sci*., 1996, *31*, pp. 785-93.
29. C. Verdon, A. Karimi, and J-L. Martin: "A Study of High Oxy-Fuel Thermally Sprayed Tungsten Carbide Based Coatings. Part 1: Microstructures," *Mater. Sci. Eng*., *A245*, 1998, pp. 11-24.
30. C-J. Li, A. Ohmori, and Y. Harada: "Formation of an Amorphous Phase in Thermally Sprayed WC-Co," *J. Therm. Spray Technol*., 1996, *5*(1), pp. 69-73.
31. M.E. Vinayo, F. Kassabji, J. Guyonnet, and P. Fauchais: "Plasma Sprayed WC-Co Coatings: Influence of Spray Conditions (Atmospheric and Low Pressure Plasma Spraying) on the Crystal Structure, Porosity, and Hardness," *J. Vac. Sci. Technol*., 1985, *A3*(6), pp. 2483-89.
32. T.B. Massalski, *Binary Alloy Phase Diagram*, 2nd ed., ASM International, Materials Park, OH, 1990.
33. W.D. Swank, J.R. Fincke, and D.C. Haggard: "HVOF Gas Flow Field Characteristics" in *Thermal Spray Industrial Applications,* C.C. Berndt and S. Sampath, ed., ASM International, Materials Park, OH, 1994, pp. 313-18.
34. W.C. Strahle: *An Introduction to Combustion*, Gordon & Breach, Amsterdam, Netherlands, 1996, pp. 26-52.
35. G.H. Geiger and D.R. Poirier: *Transport Phenomena in Metallurgy,* Addison Wesley, London, UK, 1973, pp. 163-65.
36. A.F. Guillermet: "Thermodynamic Properties of the Co-W-C System," *Metall. Trans. A*, 1989, *20A(*5), pp. 935-56.
37. H.E. Exner: "Physical and Chemical Nature of Cemented Carbides," *Int. Metals Rev.*, 1979, *24*(4), pp. 149-73.
38. Y. Arata, A. Ohmori, and E. Gofuku: "WC-Co High Energy Thermal Sprayed Coatings: Structures and Mechanical Properties," *Trans. JWRI*, 1985, *14*(2), pp. 67-73.
39. C-J. Liu, H. Yang, and H. Li: "Effect of Gas Conditions on HVOF Flame and Properties of WC-Co Coatings," *Mater. Mfg. Processes*, 1999, *14*(3), pp. 383-95.
40. R. Schwetzke and H. Kreye: "Microstructure and Properties of Tungsten Carbide Coatings Sprayed With Various HVOF Spray Systems" in *Thermal Spray: Meeting the Challenges of the 21st Century*, C. Coddet, ed., ASM International, Materials Park, OH, 1998, pp. 187-92.
41. W.J. Jarosinski, M.F. Gruninger, and C.H. Londry: "Characterization of Tungsten Carbide Cobalt Powders and HVOF Coatings" in *Thermal Spray: Research, Design, and Application*s, C.C. Berndt and T.F. Bernecki, ed., ASM International, Materials Park, OH, 1993, pp. 153-57.
42. S.Y. Hwang, B.G. Seong, and M.C. Kim: "Characterization of WC-Co Coatings Using HP/HVOF Process" in *Thermal Spray: Practical Solutions for Engineering Problems*, C.C. Berndt, ed., ASM International, Materials Park, OH, 1996, pp. 107-12.